Oxygen and silicon point defects in $Al_{0.65}Ga_{0.35}N$

Joshua S. Harris, Benjamin E. Gaddy, Ramón Collazo, Zlatko Sitar, and Douglas L. Irving

Department of Materials Science and Engineering, North Carolina State University, Raleigh, North Carolina 27695, USA

The formation energies of oxygen and silicon impurities have been examined explicitly in $Al_{0.65}Ga_{0.35}N$ using hybrid exchange-correlation density-functional theory simulations. Both impurities were initialized in on-site substitutional and off-site *DX* configurations in a range of charge states. The O_N^{+1} donor was found to always relax into an on-site configuration, and its formation energy is relatively independent of local chemistry (the configuration of Al and Ga atoms surrounding the defect). By contrast, the O_N^{-1} acceptor almost always relaxes into a *DX* configuration, with a formation energy that is strongly dependent on local chemistry. The differences in formation energy of distinct O_N^{-1} defect configurations are understood through the interplay of two qualitative trends in the types of nearest-neighbor bonds (O-Al or O-Ga), as well as the subtler influence of the lengths of the O-Al bonds. Knowledge of O_N^{-1} formation energies as well as the relative frequencies of sites with different local chemistry allows one to compute the relative site occupancies of O_N^{-1}. Because the thermodynamic transition levels associated with different defect configurations are unique, the O_N *DX* transition is associated with multiple defect levels. Si_{III}, where III represents the group III cation of Al or Ga, provides an interesting counterexample. Si_{III}^{+1} is predicted to be the dominant charge state across the entire band gap of $Al_{0.65}Ga_{0.35}N$, and little dependence of the formation energy on the composition of nearby cation sites was found. This is explained by the fact that the first-nearest neighbors are all of the same species (N), so the local environment is similar to a bulk III nitride, in which on-site Si_{III}^{+1} is stable across the same Fermi level range (i.e., below the band gap of $Al_{0.65}Ga_{0.35}N$). Thus, the trends in the energetics of O_N and Si_{III} in $Al_{0.65}Ga_{0.35}N$ are both determined by the chemistry of the four nearest-neighbor sites surrounding the defect site.

I. INTRODUCTION

Due to its direct tunable band gap, aluminum gallium nitride ($Al_xGa_{1-x}N$) is an attractive material for deep ultraviolet light sources such as light emitting diodes and laser diodes, with applications ranging from sterilization to photolithography [1,2]. In addition to its applications in optoelectronics, $Al_xGa_{1-x}N$ is also a candidate material for next-generation power electronics because of its substantial Baliga figure of merit [3]. Al-rich AlGaN is of particular interest due to its low lattice mismatch and dislocation density when grown on AlN single-crystal substrates versus heterogenous growth on non-native substrates [4,5]. Such high quality films are essential for achieving the conductivities and optical efficiencies necessary for UVC optoelectronic devices [6]. Equally essential is the control of electrical properties via doping. The distribution of point defects can be engineered during growth via various routes, such as chemical potential control [7] or Fermi level control [8,9]. Each of these routes requires a detailed understanding of the energetics of relevant point defects, which ultimately determines how defect populations will respond when a control parameter is varied. This study uses the hybrid exchange-correlation functionals within the first-principles density-functional theory (DFT) framework to understand the defect energetics of oxygen (a common unintentional impurity) and silicon (a common intentional dopant) in Al-rich AlGaN. Rather than interpolating the behavior of the defects from the end members, explicit modeling of point defects in a pseudorandom $Al_{0.65}Ga_{0.35}N$ alloy supercell

is performed and compared to previous work. Before the findings are addressed, we will briefly review previous experimental and computational work on oxygen and silicon impurities in AlN, GaN, and AlGaN alloys in the following two subsections.

A. Oxygen defects in AlGaN

Oxygen is a commonly observed unintentional impurity in GaN, AlN, and AlGaN. In GaN and Ga-rich AlGaN, O substitutes directly on the N site and acts as a hydrogenic donor at all Fermi levels below the conduction band minimum (CBM). However, at high Fermi levels in AlN and Al-rich AlGaN, O forms compensating *DX* centers [10–13]. A *DX* center is a substitutional defect in which the impurity is displaced away from the regular on-site geometry while at the same time localizing additional electrons at the defect site [14]. In this displaced configuration, O_N behaves as a compensating acceptor rather than a donor, thereby limiting its effectiveness as an *n*-type dopant.

Many computational studies have explored the properties of oxygen impurities in AlN [15–24]. Park and Chadi calculated formation energies for O in GaN and AlN in an on-site configuration and two different *DX* configurations, and used linear interpolation to predict the onset of the *DX* transition level at 20 at. % Al in the alloy [21]. That study used functionals with the local density approximation (LDA), which is known to underestimate band gaps and, in turn, can affect the accuracy of formation energy calculations. The

more recent study by Gordon *et al.* uses hybrid functionals (which more accurately reproduce the band gaps of many materials, including GaN and AlN) to model O in GaN and AlN [23]. It was found that O is solely a donor in GaN, but it forms a *DX* defect in AlN. Through interpolation (including the effects of band gap bowing), the authors predict the onset of the O *DX* transition in the alloy at a composition of 61 at. % Al.

There is some disagreement in the literature over which *DX* configuration is the most stable for O in AlN. Earlier studies based on LDA functionals conclude that the most stable configuration involves a displacement of the oxygen away from the N site along the *c* axis, such that the axial bond is broken [21,22]. However, Gordon's work, based on hybrid functionals, finds another configuration to be more stable, in which the O atom has been displaced such that one of the three nonaxial bonds is broken [23].

Note that none of these studies explicitly models the O defect in an AlGaN alloy environment. Those that draw conclusions about AlGaN do so by interpolating between results in GaN and AlN. In fact, only one study, by Bogusławski and Bernholc, does any explicit modeling of point defects in AlGaN alloy; but they model C, Si, and Ge [25].

B. Silicon defects in AlGaN

Silicon is commonly used as an intentional *n*-type dopant in AlN, GaN, and AlGaN alloys. Although it substitutes on the cation site, the silicon impurity has many characteristics which make it an interesting parallel to the oxygen impurity in AlGaN. Like O, Si acts as a hydrogenic donor in GaN and Ga-rich AlGaN [23]. Also like O, Si transitions to a *DX* configuration at high Fermi levels in AlN, but not in GaN, indicating that the onset of *DX* behavior in $Al_xGa_{1-x}N$ is above some threshold Al content [23]. This is supported by experimental measurements of a deeper donor level in Si-doped samples, which has been associated with the *DX* transition [11,26–30]. However, this *DX* transition is shallower in the band gap of AlN for Si than for O [11]. Theoretical predictions of this onset Al content vary widely, including $x = 0.24$ [21], $x = 0.6$ [25], and $x = 0.94$ [23]. Of these predictions, that of Gordon *et al.* ($x = 0.94$) is based on hybrid functionals, which have demonstrated increased accuracy in predicting these properties as compared to traditional functionals. Experimentally, Collazo *et al.* observed a sharp increase in donor activation energy for Si-doped $Al_xGa_{1-x}N$ at $x = 0.8$, which could, in part, be due to the onset of a *DX* transition [26].

C. Overview

In this paper, the nature of oxygen and silicon point defects in $Al_{0.65}Ga_{0.35}N$ are examined via explicit modeling of their properties in various configurations in pseudorandom alloy supercells of the alloy. A number of interesting results are revealed that were only elucidated upon explicit simulation of the alloy.

The O_N^{+1} donor is always found to relax into an on-site configuration, with a formation energy which is relatively independent of local chemistry (the configuration of Al and Ga atoms surrounding the defects). By contrast, O_N^{-1} has

multiple minima in different off-site *DX* configurations. The formation energies associated with distinct configurations of O_N^{-1} are principally determined by local chemistry, through the interplay of qualitative trends in nearest-neighbor bonding. These differences in formation energy also lead to multiple thermodynamic transition levels associated with different configurations of O_N^{-1} and its nearest-neighbor cations. However, it is demonstrated that only two of these thermodynamic transition levels are relevant in realistic situations, owing to the relative populations of O_N^{-1} defects in different configurations.

Si_{III} is predicted to be a singly ionized donor across the entire band gap for this alloy composition, with little dependence on the composition of nearby cation sites. This is because the first-nearest neighbors of Si_{III} are all the same species (N), so the local chemical environment is similar to a bulk III-nitride (with lattice constants between those of AlN and GaN), in which on-site Si_{III}^{+1} is stable. Therefore, the energetics of O_N and Si_{III} in $Al_{0.65}Ga_{0.35}N$ are both determined by the chemistry of the four nearest-neighbor sites surrounding the defect site.

II. METHODS

A. Computational details

All DFT calculations were carried out within the VIENNA AB INITIO SIMULATION PACKAGE (VASP 5.3) [31–34]. The hybrid exchange-correlation functional of Heyd, Scuseria, and Ernzerhof (HSE), which includes a fraction of short-range exact Hartree-Fock exchange, was used in the calculations of defect properties in $Al_{0.65}Ga_{0.35}N$ [35,36]. Owing to the high Al content of the AlGaN alloys studied here, the fraction of exact exchange was set to $\alpha = 0.32$, which reproduced the band gap of AlN from experiment while simultaneously improving structural parameters and thermodynamic quantities [37]. In previous studies, HSE functionals have been used to predict the defect formation energies and concentrations of point defects and complexes in InN, GaN, and AlN [18,23,24,37–41].

To approximate a random solid solution, 31 Al and 17 Ga atoms were pseudorandomly distributed on the cation sublattice of a wurtzite cell to create five unique 96-atom AlGaN supercells. Note that this actually corresponds to $Al_{0.646}Ga_{0.354}N$, but we will continue to refer to the composition as $Al_{0.65}Ga_{0.35}N$ throughout this paper. A 2x2x2 *k*-point mesh and a kinetic energy cutoff of 500 eV were used for all defect calculations. Pseudopotentials were used to represent Al, Ga, N, O, and Si with 3, 3, 5, 6, and 4 explicitly modeled electrons, respectively.

Formation energies were calculated using the grand canonical formalism [42,43]. In this formalism, the formation energy of a point defect D^q, where q is the charge state, is given by

$$E_{D^q}^f = E_{D^q}^{tot} - E_{bulk}^{tot} - \sum_i n_i \mu_i + q[\mu_e + E_v] + E_{D^q}^{corr}. \quad (1)$$

In this expression, $E_{D^q}^{tot}$ and E_{bulk}^{tot} are the total energies, respectively, of a supercell containing defect D^q and of the corresponding bulk supercell, as calculated with DFT simulations. $E_{D^q}^{corr}$ is a postprocessing correction to the energy

of the defect cell, which accounts for finite-size effects in charged supercells (including image charge interactions and a potential alignment with the bulk); here, a custom variation on the method of Kumagai and Oba has been used to obtain the correction [44]. For the correction, a relative permittivity of 9.34 was used, being an interpolation between experimental permittivities of 9.70 and 9.14 for GaN and AlN, respectively [45,46]. μ_i is the chemical potential of species i, and n_i is the number of atoms of species i exchanged between the bulk and a chemical reservoir to create the defect. E_v is the valence band maximum (VBM), and μ_e is the Fermi level relative to the VBM.

Data from defect formation energy calculations is typically represented with a formation energy diagram, in which defect formation energies are plotted as a function of the Fermi level. For plotting purposes, the Fermi level is treated as a free parameter which varies across the band gap. In such a plot, the charge state of a defect is represented by the slope of the line representing its formation energy. Higher-energy charge states at a given Fermi level do not occur in appreciable concentrations; thus they are often omitted from the figure to reduce clutter. The Fermi level at which two charge states of a given defect have equal formation energies (i.e., where the slope changes) is known as the thermodynamic transition level between those two states. Thermodynamic transition levels may be thought of as defect states as represented on a vertical band diagram.

The concentration of a defect D^q is related to its defect formation energy via

$$[D^q] = N_{D^q}^{\mathrm{conf}} N_{D^q}^{\mathrm{site}} \exp\left(-\frac{E_{D^q}^f}{kT}\right), \qquad (2)$$

such that a lower formation energy results in an exponentially higher defect concentration. In this expression, $N_{D^q}^{\mathrm{conf}}$ is the number of configurations of defect D^q, $N_{D^q}^{\mathrm{site}}$ is the site density of the site on which D^q sits, k is Boltzmann's constant, and T is temperature. In principle, one can solve for the concentrations of all defects in a system (in a given environment) by solving for the Fermi level at which the charge balance condition is satisfied [39,47–50].

B. Defect geometries in Al$_{0.65}$Ga$_{0.35}$N

In a wurtzite crystal, an impurity can sit on either sublattice substitutionally or it can be displaced off the sublattice site. Figure 1 illustrates each of these possible configurations in the alloy with visualizations produced with VESTA [51]. An on-site defect sits directly on the site of the atom for which it substitutes, which is tetrahedrally coordinated to four atoms of the opposite type of the removed atom. A *DX* defect is displaced slightly of site toward one of the faces of the tetrahedron so it sits approximately between the three atoms defining that face. In a *DX-c* configuration, the defect is displaced along the c axis and sits on the tetrahedron face that is normal to the c axis. In a *DX-a* configuration, the defect is displaced roughly perpendicular to the c axis (approximately in the a plane) and sits on one of the other three faces of the tetrahedron. In a pure wurtzite crystal of the end members, the cation sites are identical, which makes the three *DX-a$_i$* configurations symmetrically equivalent.
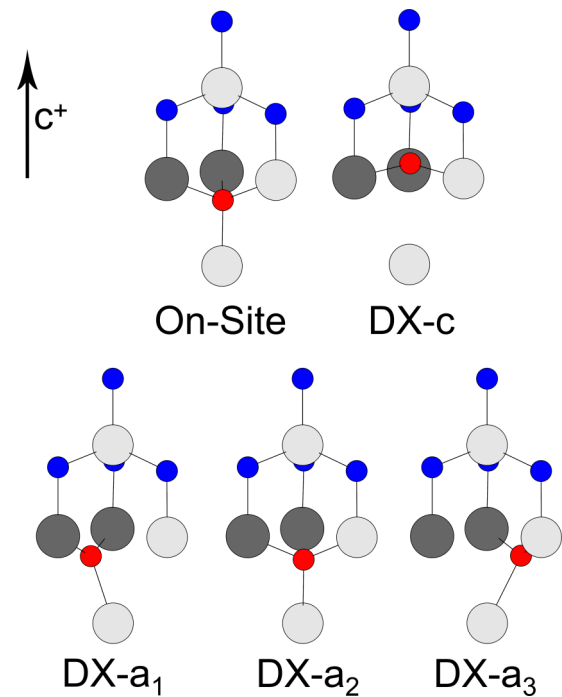
FIG. 1. Nitrogen-substitutional defect configurations in AlGaN. Light gray and dark gray spheres represent Al and Ga sites, respectively; blue spheres represent nitrogen sites and the red sphere represents a N-substitutional defect.

Substitutional defects in AlGaN are complicated by the fact that the alloy chemistry destroys the wurtzite symmetry because of the random cation site occupancy. For N-site defects in particular, the three *DX-a$_i$* configurations are no longer necessarily equivalent when looking at first-nearest neighbor chemistry, depending on which cations occupy the surrounding sites. However, this does not mean that there are no symmetrical configurations from a first-nearest neighbor perspective in the alloy. For instance, in Fig. 1, one can observe that the *DX-a$_2$* and *DX-a$_3$* configurations are equivalent because in both cases the defect is displaced away from a Ga atom and toward a tetrahedon face containing two Al atoms and one Ga atom; but the *DX-a$_1$* configuration is not equivalent to these two, since the defect is displaced away from an Al atom and toward the face containing one Al atom and two Ga atoms. As a result, discussion of defects and their distortions in an alloy requires keeping track of the local chemical configurations. To facilitate this discussion and analysis, we have established a shorthand language to capture aspects of the local chemistry in these systems.

For this purpose, the term *site coordination* (SC) will be used to denote the chemistry of the four atoms comprising the coordination tetrahedron around the nitrogen substitutional site. For instance, each defect configuration shown in Fig. 1 is in a 2-Al SC (or 2-SC), because the coordination tetrahedron is made of two Al and two Ga atoms. The term *face coordination* (FC) will be used to denote the chemistry of the three atoms comprising the tetrahedron face onto which a *DX* defect relaxes. For instance, in Fig. 1, the defects in the *DX-c* and *DX-a$_1$* configurations are in a 1-Al FC (or 1-FC), because they sit on a face containing one Al and two Ga atoms; whereas

TABLE I. Calculated bulk lattice parameters and bond lengths in GaN, AlN, and $Al_{0.65}Ga_{0.35}N$. Bond lengths are averaged over a 96-atom cell, which results in standard deviations smaller than 0.01 Å in all cases.

	GaN	AlN	$Al_{0.65}Ga_{0.35}N$
a (Å)	3.18	3.10	3.13
c (Å)	5.16	4.96	5.05
N-Ga Bond (Å)	1.94	–	1.95
N-Al Bond (Å)	–	1.89	1.89

the defects in the $DX\text{-}a_2$ and $DX\text{-}a_3$ configurations are in a 2-FC, because they sit on a face containing two Al and one Ga atoms. Furthermore, as in the examples given above, both the SC and the FC will always be specified by the number of Al atoms, with the remaining atoms being Ga. This terminology will aid the discussion of trends in the alloy, as the influence of defect configuration and local chemistry on the formation energies of O and Si defects in $Al_{0.65}Ga_{0.35}N$ is examined.

III. RESULTS AND DISCUSSION

A. Bulk $Al_{0.65}Ga_{0.35}N$ simulations

To justify the use of pseudorandomly distributed cations in a 96-atom cell, a few key bulk properties were calculated for each of the five bulk configurations. The 0 K formation enthalpy of $Al_{0.65}Ga_{0.35}N$ was found to be -2.66 eV on average with a standard deviation of only 0.03 eV. The average band gap was 5.09 eV with a standard deviation of 0.03 eV, and the standard deviation in the energy of the VBM was 0.01 eV. The a and c lattice parameters were 3.13 Å and 5.05 Å, respectively, with standard deviations less than 0.001 Å. The small amount of scatter in these bulk properties suggests that the different configurations are representative of the properties of the same random alloy. Furthermore, the small scatter in the enthalpy demonstrates an invariance of the energy to different chemical configurations, which is consistent with the formation of a random solid solution, as is found experimentally in this alloy.

Table I presents bulk lattice parameters and bond lengths as calculated in GaN, AlN, and $Al_{0.65}Ga_{0.35}N$. Bond lengths have been averaged over a 96-atom cell, resulting in standard deviations smaller than 0.01 Å in all cases. The a and c lattice parameters for $Al_{0.65}Ga_{0.35}N$ are close to the values one would expect by linearly interpolating between the a and c lattice parameters for GaN and AlN (i.e., the lattice parameters follow Vegard's law, as expected).

B. Oxygen in $Al_{0.65}Ga_{0.35}N$

A N-site substitutional defect in $Al_{0.65}Ga_{0.35}N$ is tetrahedrally coordinated to four cation sites, and may therefore exist in one of five *site coordinations* (0-SC to 4-SC). In each SC, each of the five configurations (on-site, $DX\text{-}c$, $DX\text{-}a_i$) shown in Fig. 1 must be explored. Thus, each charge state of O_N was modeled in five starting configurations in five SCs, for a total of 25 simulations per charge state. Although the computational expense is clearly high for defect simulations
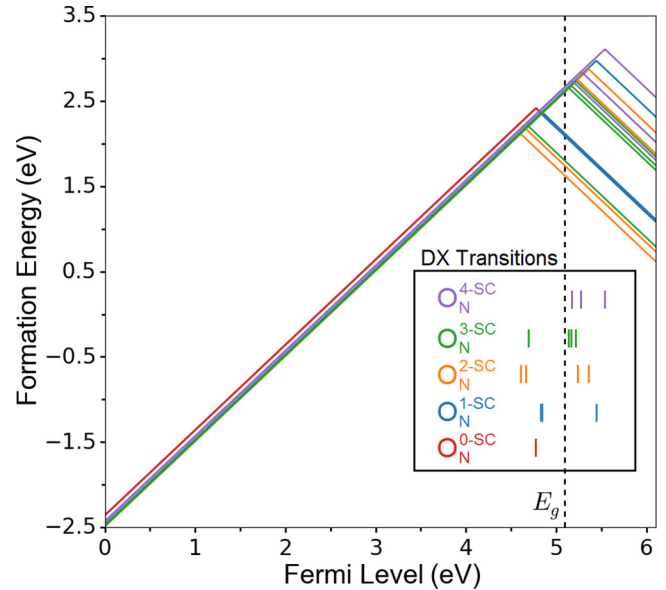
FIG. 2. Formation energy diagram for O_N in $Al_{0.65}Ga_{0.35}N$. Each of the different colors represents a unique *site coordination*, as labeled in the inset. All configurations of O_N^{-1} are represented on the plot. The Fermi level has been extended above band gap (5.09 eV, marked by a vertical dashed line) to the band gap of AlN (6.1 eV), for illustrative purposes. The markers in the inset indicate $O_N(+|-)$ transition levels associated with different O_N^{-1} configurations in each SC.

in an alloy environment, such explicit simulations allow a level of physical insight that is otherwise unavailable.

Figure 2 is a plot of O_N formation energies versus Fermi level. Note that the Fermi level in the plot extends above the band gap of $Al_{0.65}Ga_{0.35}N$ (5.09 eV), up to the band gap of AlN (6.1 eV). Each line color represents a unique SC. The formation energies of neutral O_N^0 in a given SC were found to be roughly independent of configuration (within about 0.1 eV). However, in all SCs and Fermi levels within the band gap, every configuration of O_N^0 was found to be unstable relative to other charge states, so they have been omitted from the plot.

Regardless of the initial configuration, the O_N^{+1} donor defect always relaxes to an on-site configuration in all SCs (that is, the DX configurations are not local minima of the total energy for O_N^{+1}). This is reflected in Fig. 2, where one observes a single line for the formation energy of (on-site) O_N^{+1} for each SC. Furthermore, the formation energy of O_N^{+1} is nearly independent of the SC, so the five plotted lines for O_N^{+1} in Fig. 2 almost coincide (the standard deviation is only 0.03 eV).

By contrast, the on-site configuration of the O_N^{-1} acceptor defect is a local minimum only in the 4-SC. Additionally, each of the four possible DX configurations depicted in Fig. 1 exhibit minima for O_N^{-1} in all SCs and FCs. In Fig. 2, the formation energies of all configurations of O_N^{-1} that exhibit a minimum are represented to showcase the high variability of their formation energies. Additionally, the $O_N(+|-)$ thermodynamic (DX) transition levels associated with each O_N^{-1} configuration have been marked on the plot within the inset.

In the subsections below, we will identify the mechanisms behind the observed variability of formation energies and *DX* transition levels. First, we will discuss 4-SC O_N^{-1} as a special case; then we will discuss the influence of bonding and local chemistry variations on the formation energy of O_N^{-1}, then the influence of bond lengths and, finally, we will discuss the impact of this variability on thermodynamic transition levels and fractional occupancies of different sites. We will find that the formation energy of O_N^{-1} in $Al_{0.65}Ga_{0.35}N$ is mostly determined by the local chemical environment, i.e., the chemical constituency of the four nearest-neighbor cation sites surrounding the N site on which O_N^{-1} substitutes.

1. 4-SC O_N^{-1}

A 4-SC N-site defect is completely surrounded by Al, so it is reasonable to expect it to behave similarly to a corresponding defect in AlN. As we will elucidate momentarily, the defect energetics of 4-SC O_N^{-1} support this expectation.

In Fig. 2, one observes three distinct formation energies (and correspondingly, three distinct *DX* transition levels) associated with 4-SC O_N^{-1}. The most stable (lowest formation energy) is associated with the three *DX-a_i* configurations, which have roughly identical formation energies. This degeneracy highlights the importance of local chemistry: Although the chemical constituencies of cation sites beyond the first nearest neighbors of the defect are randomized and unique for each of the three *DX-a_i* configurations, the formation energies are the same, indicating that local chemistry and bonding effects in the FC prevail over any influence from long-range disorder at our alloy composition.

The *DX-c* configuration is higher in formation energy than the *DX-a_i* configurations by about 0.2 eV. This accords with previous calculations by Gordon *et al.*, who showed that O_N^{-1} in pure AlN preferentially relaxes to a *DX-a_i* configuration, which has a lower formation energy than the *DX-c* configuration by approximately 0.2 eV in AlN [23]. Our own calculations of O_N^{-1} formation energies in pure AlN are also in agreement with those of Gordon. Thus the relative energetics of 4-SC O_N^{-1} behave similarly to those in pure AlN; in other words, the local chemistry here dominates the energetics. We will demonstrate that this is true for other SCs and FCs as well.

The on-site configuration of O_N^{-1} is unique to the 4-SC (i.e., it is not a local minimum in other SCs). Just as in AlN, it is less stable than either of the *DX* configurations. However, the formation energy of the on-site configuration is higher than that of the *DX-a_i* configurations by about 0.7 eV in $Al_{0.65}Ga_{0.35}N$, whereas the difference is about 0.5 eV in AlN, according to our calculations. Despite the slight difference, this again demonstrates that the local AlN-like environment dominates the relative energetics of 4-SC O_N^{-1}.

Finally, it should be emphasized that while all *DX* configurations of 4-SC O_N^{-1} exhibit a minimum, none of their associated *DX* transition levels are within the band gap (see Fig. 2). Although this seems to differ from AlN, in which the corresponding defect levels are within the band gap, the difference is due to the movement of the band edges as a function of Ga content rather than any effect of the local environment on the defect energetics.

TABLE II. O_N^{-1} formation energies for all SCs and FCs, relative to the most stable O_N^{-1} defect. Only the lowest formation energy is reported for locally degenerate configurations.

		O_N^{-1} formation energies (eV)

		Site coordination (n-Al SC)				
		0	1	2	3	4
	0	0.47	1.70			
Face coordination (n-Al FC)	1		0.46	1.26		
	2			0.00	1.07	
	3				0.17	1.19

2. 0-SC to 3-SC O_N^{-1}: *Bonding and local chemistry*

Local chemistry also dominates the energetics of O_N^{-1} in the 0-SC to the 3-SC, but more details are necessary to extract trends due to the local chemistry variations. In Fig. 2, for 1-SC, 2-SC, and 3-SC O_N^{-1}, one observes two distinct groups of formation energies; one group has a *DX* transition within the band gap, while in the other group the *DX* transition occurs above the CBM. The distinct groups correspond to O_N^{-1} configurations in different FCs. The formation energies of 0-SC O_N^{-1} fall into a single degenerate group, because 0-FC is the only possible *face coordination* for the 0-SC. Notably, the *DX-a_i* and *DX-c* configurations are degenerate in the 0-SC, which was not the case in the 4-SC.

Table II contains O_N^{-1} formation energies in different SCs and FCs. The values in the table are all taken relative to the most stable O_N^{-1} defect (2-SC, 2-FC). For locally degenerate configurations (same SC and FC), only the lowest formation energy is given. The values in red text represent higher energy configurations, which incidentally correspond to *DX* configurations that exhibit thermodynamic transition levels above the CBM. Notice that a given FC (rows) may originate from one of two possible SCs (columns); whereas the 0-SC and 4-SC (columns) only have one possible FC (row).

Two trends in the formation energies are observed in Table II: (1) in a given SC, O_N^{-1} prefers to maximize the number of Al atoms in its FC (i.e., in a given column, the lowest row has the lowest formation energy); and (2) in a given FC, O_N^{-1} prefers to reduce the number of Al atoms in its initial SC (i.e., in a given row, the leftmost column has the lowest formation energy).

These two trends may be qualitatively understood by appealing to a relatively simple bonding picture. To evaluate the energies of the various O_N^{-1} configurations within this model, consider the energy difference between a given *DX* configuration and its (higher energy) on-site configuration. In the on-site configuration, the defect sits within a tetrahedron of four cations, approximately equidistant from each of them with a local chemistry defined by the SC. In a *DX* configuration, the defect sits approximately on one face of the tetrahedron with a local chemistry defined by the FC. Relative to the on-site configuration, we may say that the *DX* configuration has strengthened (shortened) three bonds (with the ions forming the tetrahedron face) and broken one bond (with the ion in the remaining corner of the tetrahedron).

TABLE III. Nearest-neighbor bond lengths for the most stable O_N^{-1} defect in AlN and in each SC in $Al_{0.65}Ga_{0.35}N$. All defects are in the *DX-a* configuration, and the three bond lengths in each case are the distances to the face-coordinated cations (ordered from shortest to longest, going down each column). Highlighted cells correspond to Al-O bonds, while the rest correspond to Ga-O bonds.

(Ga,Al)-O bond lengths (Å) for O_N^{-1}					
AlN	$Al_{0.65}Ga_{0.35}N$ (n-Al SC)				
	0	1	2	3	4
1.74	1.86	1.74	1.75	1.78	1.75
1.82	1.89	1.87	1.78	1.83	1.84
1.82	1.92	1.94	1.99	1.83	1.85

The dissociation energy of Al-O bonds is almost twice that of Ga-O bonds [52]. Therefore, it is reasonable to expect that the energy of a given *DX* configuration is lower when the three bonds that are strengthened consist of as many Al-O bonds as possible (i.e., it is energetically preferable to form stronger bonds). This expectation corresponds to the first trend: In a given SC, the formation energy of O_N^{-1} is lower when the FC maximizes the number of Al atoms. Likewise, it is reasonable to expect that the energy of a given *DX* configuration is lower when the broken bond is a Ga-O bond (i.e., it is energetically preferable to break a weaker bond). This second expectation corresponds to the second trend: In a given FC, the formation energy of O_N^{-1} is lower when the SC minimizes the number of Al atoms, i.e., when the atom on the far corner of the coordination tetrahedron is Ga rather than Al.

The interplay of these two trends mostly determines the relative energetics of O_N^{-1} in $Al_{0.65}Ga_{0.35}N$. However, following the trends to their logical conclusion would lead one to predict the most stable defect to be in the 3-SC and 3-FC, which in fact is the second most stable defect (see Table II). Clearly, the two bonding trends alone are not sufficient in themselves to describe the predicted formation energies. In Sec. III B 3, we will discuss the more subtle influence of bond lengths on the defect energetics of O_N^{-1}, and we will demonstrate that the most stable defect represents the best compromise between all three influences.

3. 0-SC to 3-SC O_N^{-1}: Bond lengths and strengths

The bonding trends discussed in Sec. III B 2 rely on the assumption that the strengths of Al-O and Ga-O bonds are independent of the local bonding environment (SC and FC). However, an examination of the lengths of these bonds suggests that the bond strength may in fact vary with the SC and FC. Table III gives the bond lengths between oxygen and its three nearest-neighbor cations for the most stable O_N^{-1} defect in AlN and each SC in $Al_{0.65}Ga_{0.35}N$. All defects represented in the table are in a *DX-a* configuration, and the three bond lengths in each case are the distances to the FC cations. In the table, highlighted cells correspond to Al-O bonds, while the rest correspond to Ga-O bonds.

In our calculations of O_N^{-1} in the *DX-a* configuration in AlN, we find the corresponding Al-O bond lengths to be 1.74, 1.82, and 1.82 Å. In experiment, the Al-O tetrahedral bond length averaged over 32 aluminosilicate structures was found

TABLE IV. Relative formation energies and *DX* transition levels for the most stable defect configuration in each SC. Formation energies are reported relative to the defect with the lowest formation energy. As in Fig. 1, light gray and dark gray spheres represent Al and Ga sites, respectively; blue spheres represent nitrogen sites and the red sphere represents a N-substitutional defect.

Site coordination	0	1	2	3	4
ΔH_f^{rel}(eV)	0.47	0.46	0.00	0.17	1.19
E_{therm}(eV)	4.77	4.83	4.60	4.69	5.17

to be 1.76 Å with a standard deviation of 0.001 Å [53], and Al-O distances of 1.75 Å were recently measured in ultrathin oxide films on on AlN substrates [54]. The implication is that O_N^{-1} in the *DX-a* configuration in AlN has one Al-O bond with a nearly ideal length, and two Al-O bonds with longer than ideal lengths. These bond lengths in AlN are comparable to the Al-O bond lengths for 4-SC and 3-SC O_N^{-1} in $Al_{0.65}Ga_{0.35}N$ (the two rightmost columns in Table III), which also feature one bond close to the ideal Al-O bond length and two longer bonds.

By contrast, the Al-O bond lengths for 2-SC (2-FC) O_N^{-1} are both close to the ideal Al-O bond length. As a rule of thumb, shorter bonds are stronger bonds, indicating that the 2-SC has two strong Al-O bonds as opposed to one in the 3-SC. The strengthening of an Al-O bond comes at the expense of weakening the already weaker Ga-O bond. This bond strengthening effect is enough to perturb the bonding trends identified in Sec. III B 2, making O_N^{-1} more stable in the 2-SC than in the 3-SC, despite the corresponding change in FC.

4. Thermodynamic transitions and fractional occupancy

In Fig. 2, one observes many different thermodynamic transitions associated with the varying local chemistry around O_N^{-1}. Because of the low variability in the O_N^{+1} formation energies, differences between the $O_N(+|-)$ thermodynamic (*DX*) transition levels largely correlate with differences in the O_N^{-1} formation energies. Table IV provides the relative formation energies and *DX* transition levels for the most stable defect configuration in each SC. Each formation energy in Table IV has a corresponding entry in Table II. Each image in the first row of the table shows the O_N^{-1} defect configuration associated with the data below it. The entries in red (for the 4-SC) indicate that the defect does not exhibit a *DX* transition level within the band gap; it is above the CBM (5.09 eV).

In Table IV, we can observe the interplay of the two qualitative bonding trends and the bond strengthening effect discussed in the previous two sections. In each SC (table column), the most stable defect has maximized the number of aluminum atoms in its FC, and the remaining (unbonded) corner of the coordination tetrahedron is always a Ga ion where the SC allows it. The most stable defect is found in the

TABLE V. Relative site density and O_N^{-1} occupation probability for nitrogen sites in $Al_{0.65}Ga_{0.35}N$ with different *site coordinations*. Nondegenerate defect configurations have been taken into account in the calculation of the site occupancies. Thermodynamic transition levels corresponding to Table IV have been reproduced here for easy reference.

	Site coordination (n-Al SC)	Relative site density	O_N^{-1} Occupancy at 1400 K	E_{therm}(eV)
	0	0.016	0.003	4.77
	1	0.115	0.013	4.83
	2	0.314	0.800	4.60
	3	0.382	0.184	4.69
	4	0.174	0.000	5.17
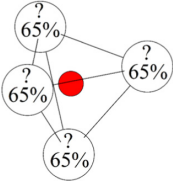
2-SC and 2-FC, representing the best compromise between the two bonding trends and the bond strengthening effect.

It is interesting that all three trends are determined by the local chemistry around the defect site. The composition of the alloy beyond the four nearest-neighbor cation sites seems to play only a second order role in the defect energetics, causing variations of at most 0.1 eV in the formation energies of locally degenerate defect configurations (which is smaller than the thermal energy at typical growth temperatures). In a given SC, only one configuration or set of degenerate configurations is stable. Thus it makes sense to consider the proportion of O_N^{-1} defects in each SC, i.e., the fractional occupancy of sites with different SCs. Fractional site occupancies at a given temperature can be computed with Eq. (2) in conjunction with our data.

Table V summarizes the results of such a calculation. Here, site density has been defined as the likelihood of choosing a N site with a given SC, if a N site is chosen at random; it is calculated probabilistically, based on the cation stoichiometry. On a site with a given SC, O_N^{-1} may take on multiple configurations, as described above. These configurations have been taken into account in the calculation of fractional site occupancies, but the formation energies of locally degenerate configurations (same SC and FC) have been averaged over the available data in order to minimize the influence of second-order effects.

Table V reveals that at 1400 K (a common temperature for epitaxial growth by MOCVD [6]) O_N^{-1} will mostly occupy sites with 3-SC or 2-SC. Although sites with 3-SC are more ubiquitous for this composition, O_N^{-1} is more likely to occupy sites with 2-SC because its formation energy is lower in the latter. After quenching to a low temperature, the relative populations of O_N on these sites may remain at their high temperature values if the oxygen ions are kinetically hindered from diffusing between sites with different SC. The thermodynamic transition levels associated with 3-SC and 2-SC are close but not identical (approximately 90 meV apart). We may therefore expect to observe multiple defect levels in the band gap associated with an $O_N(+|-)$ *DX* transition, separated by about 90 meV assuming no other defects or defect complexes interfere. This conclusion is uniquely the result of the locally random environment, and could not have been reached by interpolating between the results of simulations in AlN and GaN.

The relative site densities given in Table V apply regardless of the total concentration of O_N^{-1} defects, but they may not be measurable unless this concentration is above detection levels. Depending on experimental conditions (chemical potentials

and Fermi level), the on-site and *DX* configurations may not be the only possibilities for oxygen. For example, on-site O_N^{+1} will predominate if the Fermi level and concentration of oxygen are low. The presence of $V_{III}+nO_N$ complexes [55] may also compete with the formation of O_N^{-1} and push it to low concentrations, depending on the Fermi level and chemical potentials. Multimember complexes would be expected to be more likely when impurity concentrations are high due to their stronger dependence on the chemical potential as compared to the singular defects, as was shown for multimember silicon-vacancy complexes in AlN [24]. With this caveat in mind, the results given in Table V are relevant to measurement when a significant population of O_N^{-1} defects is present.

C. Silicon in $Al_{0.65}Ga_{0.35}N$

In AlN, oxygen forms an anion-site substitutional donor which exhibits a *DX* transition approximately 550 meV below the CBM. Silicon in AlN forms a cation-site substitutional donor which exhibits a *DX* transition approximately 200 meV below the CBM. Such a comparison of these two defects reveals that Si_{III} provides an interesting counterexample to O_N in AlGaN, where III refers to the general cation site (Al or Ga).

Figure 3 is a formation energy diagram for Si_{III} in $Al_{0.65}Ga_{0.35}N$. As in Fig. 2, the Fermi level in the plot extends above the band gap of $Al_{0.65}Ga_{0.35}N$ (5.09 eV), up to the band gap of AlN (6.1 eV). Both cation-site substitutional defects, Si_{Ga} and Si_{Al}, exhibit the same type of behavior and have a dependence on the Al or Ga chemical potentials. For simplicity, we have defined the cation chemical potentials such that Si_{Ga} and Si_{Al} are on equal footing, and we label the (Al or Ga) cation substitutional defect Si_{III}. Each line in Fig. 3 corresponds to data from a simulation in a unique bulk environment. Because the first-nearest neighbors of cation sites are all N atoms, changing the bulk configuration around a cation-site defect only affects the chemistry of second nearest neighbors and beyond.

With all of this in mind, some details in Figure 3 are immediately of note. First, there is no *DX* transition inside the band gap: Si_{III} is a hydrogenic donor across the entire band gap in $Al_{0.65}Ga_{0.35}N$. This agrees with a recent theoretical prediction by Gordon *et al.* (discussed in the introduction) and obtained via interpolation [23].

The second noteworthy feature is that the formation energies of Si_{III}^{+1} and Si_{III}^{-1} with different cation configurations are tightly clustered together (they each vary within a range of
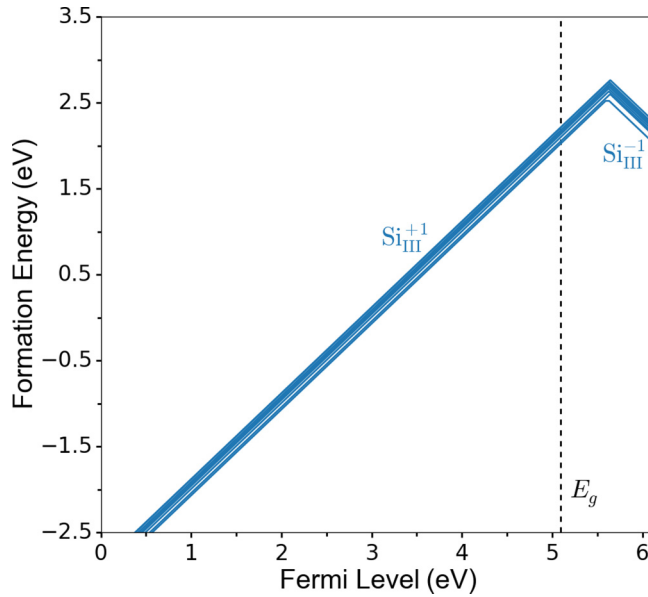
FIG. 3. Formation energy diagram for Si_{III}, a silicon substitutional on a cation site, in $Al_{0.65}Ga_{0.35}N$. Each line corresponds to data from a simulation in a unique bulk environment (cation configuration). The Fermi level has been extended above band gap (5.09 eV, marked by a vertical dashed line) to the band gap of AlN (6.1 eV) for illustrative purposes.

about 0.25 eV). This is because both charge states energetically prefer an on-site substitutional configuration regardless of the bulk cation configuration. For Si_{III}^{+1}, the DX-a_i and DX-c configurations are not local minima in the total energy landscape (the same is true of Si_{Al}^{+1} in AlN). For Si_{III}^{-1}, the DX-a_i configurations exhibit minima, but they have higher formation energies than the on-site configurations with the same bulk cation configuration. In AlN, the DX-a configuration of Si_{III}^{-1} is actually more energetically favorable than the on-site configuration; however, in GaN, the on-site configuration is more favorable (although neither configuration is stable, nor leads to a thermodynamic transition state, within the band gap in GaN). This suggests that there is some Al concentration (higher than 65%) above which the DX-a_i configurations become favorable, and below which the on-site configuration is favorable. The DX-a_i configurations of Si_{III}^{-1} are not represented in Fig. 3, since they are unfavorable relative to the on-site configuration. The DX-c configuration of Si_{III}^{-1} was not found to exhibit a minimum in GaN, AlN, or $Al_{0.65}Ga_{0.35}N$.

Finally, unlike O_N, the (above band gap) transition levels of Si_{III} exhibit little variability as a function of cation configuration. In fact, because the Si_{III}^{+1} and Si_{III}^{-1} formation energies exhibit roughly the same variation with cation configuration, the variation of the $(+|-)$ transition levels is about an order of magnitude smaller than the variation in the formation energies. The $Si_{III}(+|-)$ transition levels vary within a range of about 0.02 eV, with an average of 5.63 eV. The lone outlier (the configuration with the lowest Si_{III}^{-1} formation energy, which features a narrow range of stability for the neutral Si_{III}^0 defect) exhibits a $(+|0)$ transition at 5.59 eV and a $(0|-)$ transition at 5.63 eV.

Above, we have shown that the formation energy for the comparable O_N^{-1} defect is predominantly influenced by first-nearest-neighbor chemistry, whereas second- and higher nearest neighbors play a second-order role. Similarly, the defect energetics of Si_{III}^{+1} are also dominated by first-nearest neighbors, but because it sits on the cation site, all of the first-nearest neighbors are the same species (nitrogen). As a result, the configuration of the surrounding bulk material has little effect on the formation energy of Si_{III}^{+1}. This helps to illustrate the key role played by local chemistry in the energetics of defects in AlGaN.

It is worth mentioning that second-nearest-neighbor chemistry has been found to play a role in the energetics of Si_{III}^{-1} in previous work. There is an additional DX configuration of Si_{III}^{-1} that exhibits a minimum in which the Si atom sits substitutionally on the cation site, but a N atom is displaced away from its site along the c axis so it sits between three cation sites. Bogusławski and Bernholc used explicit alloy modeling to demonstrate that the formation energy of this configuration of Si_{III}^{-1} varies within a range of about 0.4 eV depending on whether those cation sites are occupied by Al, Ga, or some combination [25]. In our calculations, the formation energies of Si_{III}^{-1} in the DX-a_i configurations vary within a range of about 0.14 eV with different cation configurations. In AlN, we found the Bogusławski and Bernholc configuration to be unfavorable relative to the DX-a configuration when simulated with hybrid functionals. Due to the extensive computational cost for the current simulations, as well as the fact that the Si_{III}^{-1} configurations are above band gap for our alloy composition, we did not simulate this DX configuration.

With that said, based on our analysis of oxygen and its dependence on local chemistry, we hypothesize that the configuration of Bogusławski and Bernholc could be more susceptible to second-nearest-neighbor chemistry variations. The Al-N and Ga-N bond strengths are different, and would influence the energy required to displace the N atom. There is already a change in the favorable site for the ionized acceptor going from GaN (on-site) to AlN (DX-a_i) and, without explicit simulation, there is no reason to eliminate this configuration from consideration in Al-rich alloys. If present, the DX configuration of Bogusławski and Bernholc could lead to an increased variation in the formation energies of the favorable acceptor and the associated DX thermodynamic transition levels, possibly on the same order as the variation in O_N formation energies and DX transition levels (0.1–0.2 eV). We would expect this to be most important for Si_{III} in AlGaN at higher Al concentrations (above 85 %Al), where the various Si_{III}^{-1} configurations become favorable and the variability of these states may be evident from experimental measurements.

IV. CONCLUSION

The point defect energetics of a substitutional oxygen impurity in $Al_{0.65}Ga_{0.35}N$ have been examined in great detail using explicit DFT simulations of O_N in a set of 96-atom pseudorandom alloy supercells. We found that O_N^{+1} always relaxes to an on-site configuration with a formation energy that is relatively independent of the local alloy chemistry around the defect site. O_N^0 can relax into multiple configurations in

a given SC, but they all have similar formation energies and none of them are stable relative to other charge states.

O_N^{-1} generally relaxes into a *DX* configuration in a given SC, and the relative formation energies of the various possible *DX* configurations depend on the chemistry of the four nearest-neighbor cation sites. In the alloy studied here, the influence of local chemistry on the relative order of formation energies of O_N^{-1} is evident via three qualitative trends: maximizing the number of Al ions in the defect's FC, minimizing the number of Al ions in its SC, and strengthening Al-O bonds over Ga-O bonds in each FC. However, these qualitative rules of thumb are not mutually exclusive, and it is the interplay of all three effects which ultimately determines the favorability of a given O_N^{-1} defect. Second-nearest neighbors and beyond play a second-order role in the defect energetics of O_N^{-1}.

Relative site occupancies were calculated based on relative site densities and formation energies of O_N^{-1} in all possible configurations (SCs and FCs). O_N^{-1} was found to preferentially occupy sites with 2-SC, with some probability of occupying sites with 3-SC at reasonable growth temperatures. Because the thermodynamic transition levels associated with these SCs and FCs are not identical, this leads to the possibility that multiple defect levels associated with an $O_N(+|-)$ *DX* transition may be observed within the band gap when this defect is above detection limits.

Finally, we examined Si_{III} as an interesting counterexample. Si_{III}^{+1} was found to be the only stable charge state, with no *DX* transition predicted inside the band gap in $Al_{0.65}Ga_{0.35}N$. Si_{III}^{+1} always relaxes to an on-site configuration, regardless of its initial configuration, with little variation of the formation energy as a function of the distribution of second-nearest-neighbor cations.

This too is explained by the local chemistry surrounding the defect sites. The defect energetics of O_N^{-1} are dominated by the chemistry of the first-nearest-neighbor cations, which can be either Al or Ga. By contrast, the first-nearest neighbors of Si_{III}^{+1} are all N atoms, and therefore the defect behaves as it would in AlN or GaN. Therefore, first-nearest-neighbor chemistry dominates the behavior of both of these defects in $Al_{0.65}Ga_{0.35}N$.

[1] J. R. Grandusky, S. R. Gibb, M. C. Mendrick, C. Moe, M. Wraback, and L. J. Schowalter, Appl. Phys. Express **4**, 082101 (2011).

[2] J. Xie, S. Mita, Z. Bryan, W. Guo, L. Hussey, B. Moody, R. Schlesser, R. Kirste, M. Gerhold, R. Collazo, and Z. Sitar, Appl. Phys. Lett. **102**, 171102 (2013).

[3] J. Y. Tsao, S. Chowdhury, M. A. Hollis, D. Jena, N. M. Johnson, K. A. Jones, R. J. Kaplar, S. Rajan, C. G. Van de Walle, E. Bellotti, C. L. Chua, R. Collazo, M. E. Coltrin, J. A. Cooper, K. R. Evans, S. Graham, E. R. Grotjohn, E. R. Heller, M. Higashiwaki, M. S. Islam, P. W. Juodawlkis, M. A. Khan, A. D. Koehler, J. H. Leach, U. K. Mishra, R. J. Nemanich, R. C. N. Pilawa-Podgurski, J. B. Shealy, Z. Sitar, M. J. Tadjer, A. F. Witulski, M. Wraback, and J. A. Simmons, Adv. Electron. Mater. **4**, 1600501 (2017).

[4] R. Dalmau, B. Moody, R. Schlesser, S. Mita, J. Xie, M. Feneberg, B. Neuschl, K. Thonke, R. Collazo, A. Rice, J. Tweedie, and Z. Sitar, J. Electrochem. Soc. **158**, H530 (2011).

[5] M. Bickermann, B. M. Epelbaum, O. Filip, P. Heimann, M. Feneberg, S. Nagata, and A. Winnacker, Phys. Status Solidi C **7**, 1743 (2010).

[6] I. Bryan, Z. Bryan, S. Washiyama, P. Reddy, B. E. Gaddy, B. Sarkar, M. H. Breckenridge, Q. Guo, M. Bobea, J. Tweedie, S. Mita, D. L. Irving, R. Collazo, and Z. Sitar, Appl. Phys. Lett. **112**, 062102 (2018).

[7] P. Reddy, S. Washiyama, F. Kaess, R. Kirste, S. Mita, R. Collazo, and Z. Sitar, J. Appl. Phys. **122**, 245702 (2017).

[8] Z. Bryan, I. Bryan, B. E. Gaddy, P. Reddy, L. Hussey, M. Bobea, W. Guo, M. Hoffmann, R. Kirste, J. Tweedie, M.

Gerhold, D. L. Irving, Z. Sitar, and R. Collazo, Appl. Phys. Lett. **105**, 222101 (2014).

[9] P. Reddy, M. P. Hoffmann, F. Kaess, Z. Bryan, I. Bryan, M. Bobea, A. Klump, J. Tweedie, R. Kirste, S. Mita, M. Gerhold, R. Collazo, and Z. Sitar, J. Appl. Phys. **120**, 185704 (2016).

[10] M. D. McCluskey, N. M. Johnson, C. G. Van de Walle, D. P. Bour, M. Kneissl, and W. Walukiewicz, Phys. Rev. Lett. **80**, 4008 (1998).

[11] M. McCluskey, C. Van de Walle, N. Johnson, D. Bour, and M. Kneissl, International J. Mod. Phys. B **13**, 1363 (1999).

[12] V. Soltamov, I. Ilyin, A. Soltamova, E. Mokhov, and P. Baranov, J. Appl. Phys. **107**, 113515 (2010).

[13] V. Soltamov, I. Ilyin, A. Soltamova, D. Tolmachev, E. Mokhov, and P. Baranov, Diamond Relat. Mater. **20**, 1085 (2011).

[14] T. N. Morgan, Phys. Rev. B **34**, 2664 (1986).

[15] C. Stampfl and C. G. Van de Walle, Appl. Phys. Lett. **72**, 459 (1998).

[16] C. Stampfl, J. Neugebauer, and C. G. Van de Walle, Mater. Sci. Eng. B **59**, 253 (1999).

[17] C. Stampfl and C. G. Van de Walle, Phys. Rev. B **65**, 155212 (2002).

[18] L. Silvestri, K. Dunn, S. Prawer, and F. Ladouceur, Europhys. Lett. **98**, 36003 (2012).

[19] T. Mattila and R. M. Nieminen, Phys. Rev. B **55**, 9571 (1997).

[20] C. G. Van de Walle, C. Stampfl, and J. Neugebauer, J. Cryst. Growth **189**, 505 (1998).

[21] C. H. Park and D. J. Chadi, Phys. Rev. B **55**, 12995 (1997).

[22] C. G. Van de Walle, Phys. Rev. B **57**, R2033 (1998).

[23] L. Gordon, J. L. Lyons, A. Janotti, and C. G. Van de Walle, Phys. Rev. B **89**, 085204 (2014).

[24] J. S. Harris, J. N. Baker, B. E. Gaddy, I. Bryan, Z. Bryan, K. J. Mirrielees, P. Reddy, R. Collazo, Z. Sitar, and D. L. Irving, Appl. Phys. Lett. **112**, 152101 (2018).

[25] P. Bogusławski and J. Bernholc, Phys. Rev. B **56**, 9496 (1997).

[26] R. Collazo, S. Mita, J. Xie, A. Rice, J. Tweedie, R. Dalmau, and Z. Sitar, Phys. Status Solidi C **8**, 2031 (2011).

[27] R. Zeisel, M. W. Bayerl, S. T. B. Goennenwein, R. Dimitrov, O. Ambacher, M. S. Brandt, and M. Stutzmann, Phys. Rev. B **61**, R16283(R) (2000).

[28] S. Goennenwein, R. Zeisel, O. Ambacher, M. Brandt, M. Stutzmann, and S. Baldovino, Appl. Phys. Lett. **79**, 2396 (2001).

[29] N. Son, M. Bickermann, and E. Janzén, Appl. Phys. Lett. **98**, 092104 (2011).

[30] C. Skierbiszewski, T. Suski, M. Leszczynski, M. Shin, M. Skowronski, M. Bremser, and R. Davis, Appl. Phys. Lett. **74**, 3833 (1999).

[31] G. Kresse and J. Furthmüller, Comput. Mater. Sci. **6**, 15 (1996).

[32] G. Kresse and J. Furthmüller, Phys. Rev. B **54**, 11169 (1996).

[33] G. Kresse and J. Hafner, Phys. Rev. B **49**, 14251 (1994).

[34] G. Kresse and J. Hafner, Phys. Rev. B **47**, 558 (1993).

[35] J. Heyd, G. E. Scuseria, and M. Ernzerhof, J. Chem. Phys. **124**, 219906 (2006).

[36] J. Heyd, G. E. Scuseria, and M. Ernzerhof, J. Chem. Phys. **118**, 8207 (2003).

[37] R. Collazo, J. Xie, B. E. Gaddy, Z. Bryan, R. Kirste, M. Hoffmann, R. Dalmau, B. Moody, Y. Kumagai, T. Nagashima, Y. Kubota, T. Kinoshita, A. Koukitu, D. L. Irving, and Z. Sitar, Appl. Phys. Lett. **100**, 191914 (2012).

[38] B. E. Gaddy, Z. Bryan, I. Bryan, J. Xie, R. Dalmau, B. Moody, Y. Kumagai, T. Nagashima, Y. Kubota, T. Kinoshita, A. Koukitu, R. Kirste, Z. Sitar, R. Collazo, and D. L. Irving, Appl. Phys. Lett. **104**, 202106 (2014).

[39] B. E. Gaddy, Z. Bryan, I. Bryan, R. Kirste, J. Xie, R. Dalmau, B. Moody, Y. Kumagai, T. Nagashima, Y. Kubota, T. Kinoshita, A. Koukitu, Z. Sitar, R. Collazo, and D. L. Irving, Appl. Phys. Lett. **103**, 161901 (2013).

[40] J. L. Lyons, A. Janotti, and C. G. Van de Walle, Phys. Rev. B **89**, 035204 (2014).

[41] J. L. Lyons, A. Janotti, and C. G. Van de Walle, Appl. Phys. Lett. **97**, 152108 (2010).

[42] C. G. Van de Walle and J. Neugebauer, J. Appl. Phys. **95**, 3851 (2004).

[43] C. Freysoldt, B. Grabowski, T. Hickel, J. Neugebauer, G. Kresse, A. Janotti, and C. G. Van de Walle, Rev. Mod. Phys. **86**, 253 (2014).

[44] Y. Kumagai and F. Oba, Phys. Rev. B **89**, 195205 (2014).

[45] M. E. Levinshtein, S. L. Rumyantsev, and M. S. Shur, *Properties of Advanced Semiconductor Materials: GaN, AlN, InN, BN, SiC, SiGe* (John Wiley & Sons, Hoboken, NJ, 2001).

[46] A. Collins, E. Lightowlers, and P. Dean, Phys. Rev. **158**, 833 (1967).

[47] J. N. Baker, P. C. Bowes, D. Long, A. Moballegh, J. S. Harris, E. Dickey, and D. L. Irving, Appl. Phys. Lett. **110**, 122903 (2017).

[48] P. C. Bowes, J. N. Baker, J. S. Harris, B. D. Behrhorst, and D. L. Irving, Appl. Phys. Lett. **112**, 022902 (2018).

[49] J. N. Baker, P. C. Bowes, J. S. Harris, and D. L. Irving, J. Appl. Phys. **124**, 114101 (2018).

[50] E. Sachet, C. T. Shelton, J. S. Harris, B. E. Gaddy, D. L. Irving, S. Curtarolo, B. F. Donovan, P. E. Hopkins, P. A. Sharma, A. L. Sharma, J. Ihlefeld, S. Franzen, and J.-P. Maria, Nat. Mater. **14**, 414 (2015).

[51] K. Momma and F. Izumi, J. Appl. Crystallogr. **44**, 1272 (2011).

[52] B. D. Darwent, *Bond Dissociation Energies in Simple Molecules* (National Bureau of Standards NSRDS, Gaithersburg, MD, 1970).

[53] J. B. Jones, Acta Crystallogr. Sec. B **24**, 355 (1968).

[54] J. H. Dycus, K. J. Mirrielees, E. D. Grimley, R. Kirste, S. Mita, Z. Sitar, R. Collazo, D. L. Irving, and J. M. LeBeau, ACS Appl. Mater. & Interfaces **10**, 10607 (2018).

[55] Q. Yan, A. Janotti, M. Scheffler, and C. G. Van de Walle, Appl. Phys. Lett. **105**, 111104 (2014).